Tensile-strained germanium microdisks

A. Ghrib,[1] M. El Kurdi,[1,a)] M. de Kersauson,[1] M. Prost,[1,2] S. Sauvage,[1] X. Checoury,[1]
G. Beaudoin,[3] I. Sagnes,[3] and P. Boucaud[1,b)]
[1]*Institut d'Electronique Fondamentale, CNRS-Univ. Paris Sud 11, Bâtiment 220, F-91405 Orsay, France*
[2]*STMicroelectronics, 850 rue Jean Monnet, 38920 Crolles, France*
[3]*Laboratoire de Photonique et de Nanostructures, CNRS-UPR 20, Route de Nozay 91460 Marcoussis, France*

We show that a strong tensile strain can be applied to germanium microdisks using silicon nitride stressors. The transferred strain allows one to control the direct band gap emission that is shifted from 1550 nm up to 2000 nm, corresponding to a biaxial tensile strain around 1%. Both Fabry-Perot and whispering gallery modes are evidenced by room temperature photoluminescence measurements. Quality factors up to 1350 and limited by free carrier absorption of the doped layer are observed for the whispering gallery modes. We discuss the strain profile in the microdisks as a function of the disk geometry. These tensile-strained microdisks are promising candidates to achieve Ge laser emission in compact microresonators. © 2013 AIP Publishing LLC. [http://dx.doi.org/10.1063/1.4809832]

Germanium laser emission has been recently demonstrated under optical and electrical pumping providing a new pathway to realize an optical source for silicon photonics compatible with complementary metal oxide semiconductor (C-MOS) environment.[1,2] For integration purposes, a compact structure using a microresonator as the optical cavity is highly desirable. The microresonators could take the form of microrings,[3] distributed Bragg reflector cavities,[4] photonic crystals,[5,6] or microdisks. Bulk germanium microdisks have been fabricated and whispering gallery modes have been evidenced in these structures under optical and electrical injection.[7,8] For germanium, the requirement on carrier density needed to achieve optical transparency and optical gain can be lowered by introducing tensile strain. The tensile strain decreases the energy splitting between the L valley and direct conduction Γ valley and lifts the degeneracy between heavy hole and light hole bands. The larger the tensile strain, the lower is the requirement on carrier densities to obtain optical gain.[9–12]

Different approaches have been proposed to transfer tensile strain into germanium films. The difference of thermal dilatation coefficient between germanium and silicon allows one to introduce a limited 0.25% tensile strain in germanium.[13] The growth on buffer layers with a lattice constant larger than the one of germanium like $In_{1-x}Ga_xAs$ or GeSn can lead to the transfer of high biaxial tensile strain.[14–17] Another approach to achieve tensile strain is based on the use of micromechanical strain engineering or the use of an external stressor.[4,18–20] The use of silicon nitride as a stressor layer is certainly a very attractive possibility due to its compatibility with a C-MOS processing environment and the flexibility that it offers to control the stress transfer and to achieve high tensile strain.[21–23]

In this letter, we show that the emission of germanium microdisks can be controlled by using a silicon nitride film as a stressor. The room temperature direct band gap emission of the microdisk is red-shifted from 1550 nm up to 2000 nm after nitride encapsulation. We observe both Fabry-Perot and

whispering gallery modes in the unstrained or strained microresonators. The quality factors of the whispering gallery modes, up to 1350, are limited by the free carrier absorption of the n-doped germanium active layer. We provide an analysis of the strain profile as a function of the disk pedestal diameter and disk diameter. The increase in the post diameter allows one to enhance the average tensile strain in the whole Ge membrane.

The investigated microdisks were fabricated from germanium grown on GaAs. The growth of germanium on GaAs is performed by metal-organic vapor phase deposition using an isobutyl-germane source. During the germanium growth, an AsH_3 flow is maintained in order to prevent As desorption from the buffer layer, and to obtain *in situ* doping of n-type around 10^{19} cm^{-3} in the germanium layer. A resistivity of $1.5 \times 10^{-5} \Omega$ cm was measured on reference samples corresponding to an electron free carrier density around 10^{19} cm^{-3}. High optical quality germanium films are obtained by this method as no intermediate defect layer is present as it is the case for the growth of lattice-mismatched germanium on silicon. The germanium thickness was 300 nm, corresponding approximately to a $\lambda/2n_{eff}$ thickness for a 2000 nm wavelength (λ) with n_{eff} the effective refractive index of the confined mode. The germanium microdisks were defined by electronic lithography using a negative photoresist. The germanium was etched by inductively coupled plasma etching with C_4F_8 and SF_6 gases. Wet etching using a H_3PO_4 and HNO_3 chemistry was used to etch GaAs. The size of the post that supports the germanium microdisk is controlled by this wet etching step. A silicon nitride layer was then deposited by plasma-enhanced chemical vapor deposition. The thickness of the silicon nitride film is around 300 nm. Nitride is also deposited on the edge of the microdisk as well as on the lower interface but with a very small thickness. The deposition conditions were optimized in order to obtain a high compressive stress in the nitride layer.[22] As the nitride is free to extend laterally, it relaxes its stress and transfers tensile strain into the germanium film. The optical experiments were performed at room temperature using a microphotoluminescence set-up. The photoluminescence

a)Electronic mail: moustafa.el-kurdi@u-psud.fr
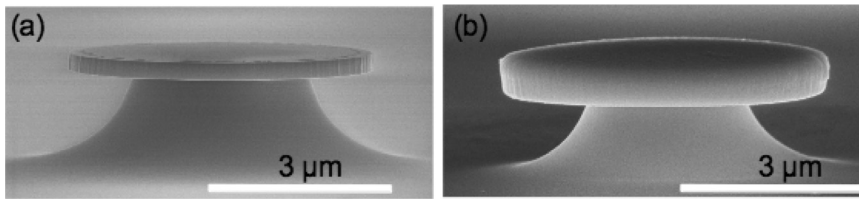b)URL: http://pages.ief.u-psud.fr/QDgroup

FIG. 1. Scanning electron microscopy images of an unstrained (a)-left and a tensile-strained (b)-right germanium microdisks. The pedestal is in GaAs while the disk is in germanium. The stressor is a silicon nitride film deposited after microdisk processing.

was excited at normal incidence using a continuous wave He-Ne laser at 632.8 nm or a pulsed laser diode at 790 nm. Optical pulses with a duration of 10 ns and a repetition time of 400 ns were used. The incident pump power on the sample is around 1 mW weakly focused on the microdisk. The optical pumping conditions were chosen in order to avoid or strongly minimize thermal heating of the microdisk.[7] The normal-incidence geometry is certainly not the optimized geometry to observe whispering gallery modes but it did not prevent us from observing a set of gallery modes. The luminescence was dispersed by a grating (600 lines/mm) monochromator and detected by an extended InGaAs array diode with a cut-off around 2100 nm.

Fig. 1 shows scanning electron microscopy (SEM) images of unstrained (a) and tensile-strained (b) microdisks. In the present experiments, the disk diameter varies between 4 and 6 μm. The same wet etching was used to process all the microdisks and consequently the diameter of the GaAs post varies between 1 and 3 μm. The post is rather Bell-shaped and the interface between GaAs and germanium is thinner than the one that can be directly observed on these SEM images. The germanium sidewalls are smooth ensuring limited losses by surface roughness for whispering gallery modes. After nitride encapsulation, the strain is strong enough to induce a significant bending of the microdisks. The observed bending of the disk is a consequence of the difference in silicon nitride thickness between the surface and the bottom of the microdisk. As discussed below, this bending is well reproduced by the finite element modeling of microdisk deformation.

Fig. 2(a) shows a comparison between the room temperature photoluminescence of an unstrained microdisk and a strained microdisk. The direct band gap recombination of bulk doped Ge grown on GaAs is maximum around 1545 nm while the maximum of the indirect band gap recombination is observed around 1800 nm. The modulation of the emission between 1800 and 1940 nm is due to water vapor absorption. For the microdisk, the direct band gap and indirect bad gap recombinations are modulated by a series of broad resonances that are emphasized in Fig. 2(a) by the vertical dashed lines for the unstrained microdisk. We associate these resonances to Fabry-Perot modes along the disk diameter for the following reasons.[24] We have observed the same type of modes in terms of quality factor and free spectral range in straight waveguides with the same width. In the latter case, there is by construction no whispering gallery modes. Moreover, the spectral positions of the broad resonances are in excellent agreement with those that can be calculated if we account for the spectral index dispersion of germanium. The result of the calculation is shown as blue dots in Fig. 2(a). The broadening of these resonances is limited by the losses due to reflectivity at the Ge/air interface, the free

carrier absorption, and the scattering and radiation losses due to the pedestal and the interfaces. A careful look at the spectra shows that additional modes are superimposed on the broad resonances. Fig. 2(b) shows a zoom of the spectrum around 1740 nm. Much narrower modes are observed and are attributed to whispering gallery modes. We associate the reduced visibility of the whispering gallery modes to the normal-incidence collection geometry. The mode at 1740 nm has a full width at half maximum around 1.3 nm, corresponding to a Q factor around 1350. This value is larger than those previously reported for microdisks with undoped germanium.[7,8] If we suppose that the Q factor is limited by the free carrier absorption according to $Q_{abs} = 2\pi n_{eff}/\alpha\lambda$, where α is the free carrier absorption, λ the resonance wavelength, and $n_{eff} \sim 3.5$ the effective index of the guided mode, one deduces a free carrier absorption coefficient around 95 cm^{-1}. This value is consistent with a 1.4×10^{19} cm^{-3} doping of the germanium film following the formula $\alpha = 3.4 \times 10^{-25} N_{3D} \lambda^{2.25}$ for n-doped germanium, where N_{3D} is the doping density and λ the resonance wavelength.[9,10] Many whispering gallery modes labeled by their azimuthal and radial numbers can be calculated both for transverse-electric and transverse magnetic polarizations for this microdisk diameter. The assignment of the observed modes to specific polarization and
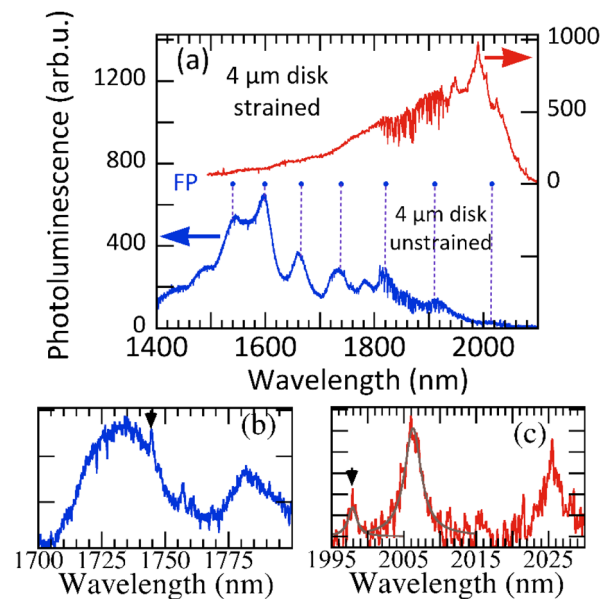

FIG. 2. (a) Room temperature photoluminescence spectra of an unstrained (bottom curve) or tensile-strained (top curve) 4 μm diameter microdisk. The dots correspond to the calculated spectral positions of Fabry-Perot (FP) modes for the unstrained microdisk. The assignment of FP modes with the broad resonances is highlighted by the vertical dashed lines. (b) Zoom of the emission for the unstrained disk around 1740 nm. (c) Zoom of the emission for the tensile-strained disk around 2015 nm, after baseline subtraction. The grey solid curves correspond to Lorentzian fits. One observes whispering gallery modes in both structures. The Q factors for modes at 1744 and 1998 nm, indicated by arrows, are around 1350 and 1000.
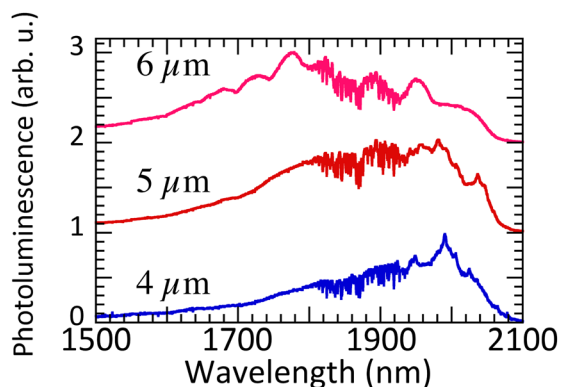
FIG. 3. Room temperature photoluminescence spectra of tensile-strained germanium microdisks for three different disk diameters. The spectra have been offset for clarity.

spatial profiles is however not straightforward as many modes are theoretically predicted, making the identification too delicate for this microdisk size. The photoluminescence of the tensile-strained microdisk is considerably shifted to long wavelength as the maximum of the emission is observed around 1990 nm. This corresponds to a significant spectral shift of about 445 nm, a signature of the large tensile strain that is present in the microdisks. As discussed below, a biaxial strain around 1% in germanium is achieved by this stress transfer method. This large shift and the broadening are a consequence of the splitting between heavy hole and light hole bands. Indeed, both bands contribute to the optical recombination and the light hole band has a much stronger energy dependence vs. strain as compared to the heavy hole band, thus pushing the recombination at long wavelength and increasing the broadening as the strain is increased. It is more difficult to observe series of Fabry-Perot resonances for highly strained microdisks, as these resonances are more easily evidenced at long wavelength away from the strong direct band gap absorption, i.e., beyond the cut-off of the detector. Moreover, the nitride film present on the edge of the microdisk can decrease the reflectivity of the interface. As for the unstrained microdisk, one can also observe narrow resonances that are again attributed to whispering gallery modes. Fig. 2(b) shows a zoom of the emission spectrum of the strained microdisk around 2010 nm after a baseline subtraction. The grey solid lines correspond to Lorentzian fits of the resonances. The peak around 1997 nm has a linewidth around 2 nm (Q factor around 1000, precision limited by signal-to-noise ratio) while the peak at 2006 nm has a

linewidth around 2.8 nm (Q factor of 700). We note that one should expect an increase of the free carrier absorption at longer wavelength following the formula for free carrier absorption given above. The lower Q factors at long wavelength follows the increase of losses at long wavelength. Note that this effect might be counterbalanced by a difference of Fermi-level pinning at the germanium-nitride interface between strained and unstrained disk leading to a change in carrier depletion and the overlap of the optical mode with the doped layers. The broadening of the whispering gallery modes increases when the pump power is increased as a consequence of an increased free carrier absorption by photo-induced carriers (electrons and holes).

Figure 3 shows the spectral dependence of the microdisk emission as a function of the disk diameter. The spectra have been offset for clarity. As expected, the spectral range periodicity of Fabry-Perot modes is decreased as the disk diameter increases. Clearly, the spectra are more red-shifted as the disk diameter decreases. For the 6 μm diameter disk, the maximum is found around 1780 nm as compared to 1990 nm for the 4 μm microdisk. Two features can explain this behavior. The nitride stressor can only transfer strain efficiently in structures with a moderate deformation resistance. The strain transfer at the interface between nitride and germanium is thus larger in structures with small pedestals. This trend was also observed for ridge waveguides as a function of the waveguide width.[22] The second feature is associated with the amplitude ratio between the heavy hole and light hole bands recombinations. At normal incidence, the amplitude of the light hole band is expected to be significantly smaller than the amplitude of the heavy hole band because of the orientation of the matrix element along the z-direction.[20,25] This ratio can, however, be modified by the scattering of light by roughness or by bending. It is likely that the scattering is modified for disks with different diameters, and the light hole recombination is more easily enhanced for disks with small diameters, thus pushing the maximum of recombination at long wavelength.

The strain profile in the germanium film is not homogeneous and several parameters have an impact on the stress transferred into the germanium. We have performed finite element modeling of the strain profile. The parameters are similar to those used in Ref. 22. Figure 4(a) shows a cross-section of the radial component of the strain field (ε_r) for a disk of 4 μm diameter with a 1 μm pedestal. A bending with a height difference of 130 nm between center and edge, as
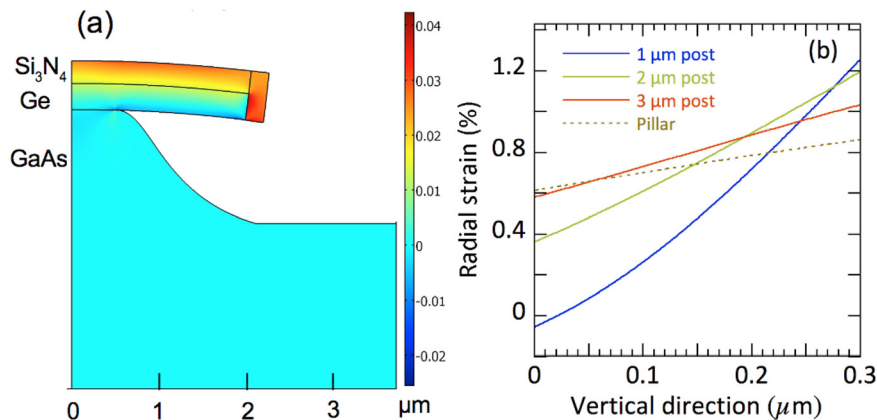

FIG. 4. Finite element modeling of the strain profile for a 4 μm diameter disk with a 1 μm pedestal. (a) Cross-section representing the radial component of the strain field. Only half of the structure is represented. The black solid lines are guides to the eye to distinguish the different layers. The color bar indicates the strain amplitude. (b) Amplitude of the strain field calculated at the disk center as a function of the vertical direction for different pedestal diameters. 0 corresponds to the interface between Ge and GaAs, 0.3 corresponds to the Ge/nitride interface.

observed experimentally, is evidenced. In germanium, the strain is maximum at the interface between the nitride and the germanium film. The finite element modeling predicts a biaxial tensile strain larger than 1% at the top interface. If we consider that the luminescence mainly stems from the first 100 nm close to the nitride surface, this value leads to a satisfying agreement for the modeling of the photoluminescence spectrum (not shown). The large broadening is essentially associated with the splitting between heavy hole an light hole bands and with the strain inhomogeneity. The modeling also reproduces the decrease of the strain field as observed in Fig. 3 when the disk diameter increases. The maximum strain is reduced for disks with a larger diameter by 0.1% and 0.25% for 6 and 7 μm (not shown) diameter disks, respectively. An important feature is that the strain decreases along the vertical direction from top to bottom and this decrease is dependent on the pedestal diameter. The deformation at the top surface is maximum for a pedestal with a small diameter. In this case, the variation of strain along the z direction is very strong and the strain can even become compressive at the bottom of the film (see Fig. 4(a)). This behavior is summarized in Fig. 4(b) which shows the dependence of the strain at the center of the disk along the z vertical direction for different pedestal diameters. The disk diameter is fixed (4 μm). The strain is indeed maximum for a 1 μm pedestal but the decrease along the z direction from top to bottom is significant. On the contrary, a pillar exhibits a lower strain amplitude at disk center but the strain field is much more homogeneous in the germanium film. A similar behavior is observed when we move away from the disk center. The pillar configuration might thus be more favorable to achieve a homogeneous large strain in a germanium disk. The larger average deformation in the whole germanium film volume is also obtained for the pillar. The strain distribution is all the more important that the band bending is expected to follow the strain profile leading to carrier accumulation in low band gap regions where surface recombinations might play an important role. If the slope of the strain variation is too high, the carriers will be confined into a narrow region with a weak overlap with the confined optical mode. It can thus significantly decrease the available optical gain. We note that since the layer is doped, the intrinsic Q factor could only be measured at optical transparency. The threshold of a microdisk laser will be reduced by increasing the overlap between the whispering gallery mode and the active gain region as well as the increase of the photon lifetime. Using disks with smaller diameters will reduce the number of confined modes and should thus enhance the coupling factor of the spontaneous emission into the mode of interest.

In conclusion, we have demonstrated that a significant tensile strain, up to 1% biaxial strain, can be applied to germanium microdisks. Fabry Perot and whispering gallery modes have been evidenced by optical measurements at room temperature with quality factors limited by the free carrier absorption of the doped layers. We have shown that a more homogeneous tensile strain and a larger volume average tensile strain could be obtained in the germanium

layer by increasing the post diameter. There might be a trade-off between the homogeneity and large average strain value and the conservation of a high Q factor for whispering gallery modes. Microdisks with smaller diameters are potential candidates to demonstrate microlaser with strained germanium.

[1]J. Liu, X. Sun, R. Camacho-Aguilera, L. C. Kimerling, and J. Michel, Opt. Lett. **35**, 679 (2010).

[2]R. E. Camacho-Aguilera, Y. Cai, N. Patel, J. T. Bessette, M. Romagnoli, L. C. Kimerling, and J. Michel, Opt. Express **20**, 11316 (2012).

[3]P. H. Lim, Y. Kobayashi, S. Takita, Y. Ishikawa, and K. Wada, Appl. Phys. Lett. **93**, 041103 (2008).

[4]D. Nam, D. Sukhdeo, S.-L. Cheng, A. Roy, K. C.-Y. Huang, M. Brongersma, Y. Nishi, and K. Saraswat, Appl. Phys. Lett. **100**, 131112 (2012).

[5]S. David, M. El Kurdi, P. Boucaud, A. Chelnokov, V. Le Thanh, D. Bouchier, and J. M. Lourtioz, Appl. Phys. Lett. **83**, 2509 (2003).

[6]T.-P. Ngo, M. El Kurdi, X. Checoury, P. Boucaud, J. F. Damlencourt, O. Kermarrec, and D. Bensahel, Appl. Phys. Lett. **93**, 241112 (2008).

[7]G. Shambat, S.-L. Cheng, J. Lu, Y. Nishi, and J. Vuckovic, Appl. Phys. Lett. **97**, 241102 (2010).

[8]S.-L. Cheng, G. Shambat, J. Lu, H.-Y. Yu, K. Saraswat, T. I. Kamins, J. Vuckovic, and Y. Nishi, Appl. Phys. Lett. **98**, 211101 (2011).

[9]J. Liu, X. Sun, D. Pan, X. Wang, L. C. Kimerling, T. L. Koch, and J. Michel, Opt. Express **15**, 11272 (2007).

[10]M. El Kurdi, G. Fishman, S. Sauvage, and P. Boucaud, J. Appl. Phys. **107**, 013710 (2010).

[11]G. Pizzi, M. Virgilio, and G. Grosso, Nanotechnology **21**, 055202 (2010).

[12]B. Dutt, D. Sukhdeo, D. Nam, B. Vulovic, Z. Yuan, and K. Saraswat, IEEE Photon. J. **4**, 2002 (2012).

[13]Y. Ishikawa, K. Wada, D. D. Cannon, J. Liu, H.-C. Luan, and L. C. Kimerling, Appl. Phys. Lett. **82**, 2044 (2003).

[14]J. Menendez and J. Kouvetakis, Appl. Phys. Lett. **85**, 1175 (2004).

[15]Y. Bai, K. E. Lee, C. Cheng, M. L. Lee, and E. A. Fitzgerald, J. Appl. Phys. **104**, 084518 (2008).

[16]Y. Huo, H. Lin, R. Chen, M. Makarova, Y. Rong, M. Li, T. I. Kamins, J. Vuckovic, and J. S. Harris, Appl. Phys. Lett. **98**, 011111 (2011).

[17]R. Jakomin, M. de Kersauson, M. El Kurdi, L. Largeau, O. Mauguin, G. Beaudoin, S. Sauvage, R. Ossikovski, G. Ndong, M. Chaigneau, I. Sagnes, and P. Boucaud, Appl. Phys. Lett. **98**, 091901 (2011).

[18]P. H. Lim, S. Park, Y. Ishikawa, and K. Wada, Opt. Express **17**, 16358 (2009).

[19]M. El Kurdi, H. Bertin, E. Martincic, M. de Kersauson, G. Fishman, S. Sauvage, A. Bosseboeuf, and P. Boucaud, Appl. Phys. Lett. **96**, 041909 (2010).

[20]J. R. Sanchez-Perez, C. Boztug, F. Chen, F. F. Sudradjat, D. M. Paskiewicz, R. Jacobson, M. G. Lagally, and R. Paiella, *Proc. Natl. Acad. Sci.* 108, 18893 (2011).

[21]D. Nam, D. Sukhdeo, A. Roy, K. Balram, S.-L. Cheng, K. C.-Y. Huang, Z. Yuan, M. Brongersma, Y. Nishi, D. Miller, and K. Saraswat, Opt. Express **19**, 25866 (2011).

[22]A. Ghrib, M. de Kersauson, M. El Kurdi, R. Jakomin, G. Beaudoin, S. Sauvage, G. Fishman, G. Ndong, M. Chaigneau, R. Ossikovski, I. Sagnes, and P. Boucaud, Appl. Phys. Lett. **100**, 201104 (2012).

[23]G. Capellini, G. Kozlowski, Y. Yamamoto, M. Lisker, C. Wenger, G. Niu, P. Zaumseil, B. Tillack, A. Ghrib, M. de Kersauson, M. El Kurdi, P. Boucaud, and T. Schroeder, J. Appl. Phys. **113**, 013513 (2013).

[24]J. S. Xia, Y. Ikegami, K. Nemoto, and Y. Shiraki, Appl. Phys. Lett. **90**, 141102 (2007).

[25]M. de Kersauson, M. El Kurdi, S. David, X. Checoury, G. Fishman, S. Sauvage, R. Jakomin, G. Beaudoin, I. Sagnes, and P. Boucaud, Opt. Express **19**, 17925 (2011).